

November 2003
 PM/03-27
 THES-TP 2003-04

Neutralino pair production in a $\gamma\gamma$ Collider[†].

G.J. Gounaris^a, J. Layssac^b, P.I. Porfyriadis^a and F.M. Renard^b

^aDepartment of Theoretical Physics, Aristotle University of Thessaloniki,
 Gr-54124, Thessaloniki, Greece.

^bPhysique Mathématique et Théorique, UMR 5825
 Université Montpellier II, F-34095 Montpellier Cedex 5.

Abstract

We present a complete 1-loop study of the process $\gamma\gamma \rightarrow \tilde{\chi}_i^0 \tilde{\chi}_j^0$ and the predicted cross section in a $\gamma\gamma$ Linear Collider. A suitable numerical code PLATONlc, valid for any set of real MSSM parameters, is released. This study and code are complementary to those suitable for Dark Matter detection through the inverse process $\tilde{\chi}_i^0 \tilde{\chi}_j^0 \rightarrow \gamma\gamma$ describing neutralino-neutralino annihilation at rest, which were presented previously. If SUSY is realized in Nature, both codes should be very helpful in future astrophysical and collider studies of the neutralino sector.

PACS numbers: 12.15.-y, 14.80.Ly

[†]Programme d'Actions Intégrées Franco-Hellenique, Platon 04100 UM

1 Introduction

A tacit candidate particle for the dominant contribution to the cold Dark Matter (DM) that apparently constitutes almost a third of the energy density of our Universe is, of course, the lightest neutralino(s) predicted in an R-parity conserving minimal supersymmetric model (MSSM) [1, 2, 3]. Provided the MSSM couplings have the appropriate values, the annihilation processes $\tilde{\chi}_1^0 \tilde{\chi}_1^0 \rightarrow \gamma\gamma$, γZ could produce observable rates of very energetic photons coming from the center of our Galaxy [4, 5, 6, 7, 8].

Such observable photon rates could be realized due to a large Wino or Higgsino component for the lightest neutralino $\tilde{\chi}_1^0$, and possibly also from resonance effects induced by the A^0 or H^0 masses [4, 5, 6, 7]. In any case, the observability of such halo galactic photons depends so strongly on the MSSM parameters, that even the non-observation of any signal could produce useful constraints.

Complementary, and in principle much more detail information on the neutralino properties could be obtained by studying $e^-e^+ \rightarrow \tilde{\chi}_i^0 \tilde{\chi}_j^0$ and $\gamma\gamma \rightarrow \tilde{\chi}_i^0 \tilde{\chi}_j^0$ at a Linear Collider (LC) [9], for any neutralino pair ($i, j = 1, \dots, 4$) accessible by the available energy. Since the first of these processes is realized already at the tree level, studying its signatures should eventually supply most of the experimentally accessible information on the neutralinos [10, 11].

Nevertheless, the study of the 1-loop process $\gamma\gamma \rightarrow \tilde{\chi}_i^0 \tilde{\chi}_j^0$ in a $\gamma\gamma$ Linear Collider ($LC_{\gamma\gamma}$) [12], is also useful, since it directly tests in an Earthy experiment, exactly the same process as in the Dark Matter (DM) searches. Compared to the DM studies, the extra advantage of Collider measurements though, is that they can be done for any neutralino pair - even unstable ones, and be performed over a considerable range of energies. Furthermore, depending on the polarizations of the e^\pm -beams and the laser photon beams, six different "cross-section-like" observables are in principle available, even if we sum over all possible helicities of the final neutralinos; see *e.g.* [13]. This is much richer than in the case of DM studies where only the unpolarized total $\tilde{\chi}_i^0 \tilde{\chi}_j^0 \rightarrow \gamma\gamma$ cross section for the cosmologically stable $\tilde{\chi}_i^0$ neutralinos, very close to threshold, is relevant.

The purpose of this work is to present such a study based on the complete set of the contributing 1-loop diagrams. In Section 2 we discuss the general properties of the amplitudes of the processes $\gamma\gamma \rightarrow \tilde{\chi}_i^0 \tilde{\chi}_j^0$ and its reverse, as well as those of the $LC_{\gamma\gamma}$ -observables, when the neutralino helicities are summed over. The results for these observables in an extensive set of MSSM benchmark models are discussed in Section 3, where the released PLATONlc code is also presented. Finally Section 4 contains the conclusions.

2 The processes $\gamma\gamma \leftrightarrow \tilde{\chi}_i^0 \tilde{\chi}_j^0$

We denote by $F_{\lambda_1, \lambda_2; \mu_1, \mu_2}^{ij}(\theta)$, the invariant amplitudes for the process $\tilde{\chi}_i^0 \tilde{\chi}_j^0 \rightarrow \gamma\gamma$ at a center-of-mass scattering angle θ . Here (λ_i, λ_j) denote the helicities of the neutralinos ($\tilde{\chi}_i^0, \tilde{\chi}_j^0$) (with $i, j = 1, \dots, 4$ being the neutralino counting indices), and (μ_1, μ_2) the helicities

ties of the photons¹. The amplitudes for the reverse process $\gamma\gamma \rightarrow \chi_i^0\chi_j^0$ are written as $\tilde{F}_{\mu_1,\mu_2;\lambda_1,\lambda_2}^{ij}(\theta)$.

Following the Jacob-Wick conventions [14], the $\chi_i^0\chi_j^0$ -fermion antisymmetry implies²

$$\begin{aligned} F_{\lambda_1,\lambda_2;\mu_1,\mu_2}^{ij}(\theta) &= (-1)^{\mu_1-\mu_2} F_{\lambda_2,\lambda_1;\mu_1,\mu_2}^{ji}(\pi-\theta) , \\ \tilde{F}_{\mu_1,\mu_2;\lambda_1,\lambda_2}^{ij}(\theta) &= (-1)^{\mu_1-\mu_2} \tilde{F}_{\mu_1,\mu_2;\lambda_2,\lambda_1}^{ji}(\pi-\theta) , \end{aligned} \quad (1)$$

while the $\gamma\gamma$ -boson symmetry requires

$$\begin{aligned} F_{\lambda_1,\lambda_2;\mu_1,\mu_2}^{ij}(\theta) &= (-1)^{\lambda_1-\lambda_2} F_{\lambda_1,\lambda_2;\mu_2,\mu_1}^{ij}(\pi-\theta) , \\ \tilde{F}_{\mu_1,\mu_2;\lambda_1,\lambda_2}^{ij}(\theta) &= (-1)^{\lambda_1-\lambda_2} \tilde{F}_{\mu_2,\mu_1;\lambda_1,\lambda_2}^{ij}(\pi-\theta) . \end{aligned} \quad (2)$$

If the MSSM breaking parameters and the Higgs parameter μ are real, then time reversal and CP invariance hold for the neutralino processes, implying also

$$\tilde{F}_{\mu_1,\mu_2;\lambda_1,\lambda_2}^{ij}(\theta) = F_{\lambda_1,\lambda_2;\mu_1,\mu_2}^{ij}(\theta) . \quad (3)$$

$$\begin{aligned} F_{-\lambda_1,-\lambda_2;-\mu_1,-\mu_2}^{ij}(\theta) &= (-1)^{\lambda_1-\lambda_2-(\mu_1-\mu_2)} \eta_i \eta_j F_{\lambda_1,\lambda_2;\mu_1,\mu_2}^{ij}(\theta) , \\ \tilde{F}_{-\mu_1,-\mu_2;-\lambda_1,-\lambda_2}^{ij}(\theta) &= (-1)^{\lambda_1-\lambda_2-(\mu_1-\mu_2)} \eta_i \eta_j \tilde{F}_{\mu_1,\mu_2;\lambda_1,\lambda_2}^{ij}(\theta) , \end{aligned} \quad (4)$$

where $\eta_j = \pm 1$ is the CP-eigenvalue of the neutralino³ $\tilde{\chi}_j^0$.

Combining (1, 2, 4), we get

$$\begin{aligned} F_{\lambda_1\lambda_2;\mu_1\mu_2}^{ij}(\theta) &= (-1)^{\mu_1-\mu_2+\lambda_2-\lambda_1} F_{\lambda_2\lambda_1;\mu_2\mu_1}^{ji}(\theta) = \eta_i \eta_j F_{-\lambda_2,-\lambda_1;-\mu_2,-\mu_1}^{ji}(\theta) , \\ \tilde{F}_{\mu_1\mu_2;\lambda_1\lambda_2}^{ij}(\theta) &= (-1)^{\mu_1-\mu_2+\lambda_2-\lambda_1} \tilde{F}_{\mu_2\mu_1;\lambda_2\lambda_1}^{ji}(\theta) = \eta_i \eta_j \tilde{F}_{-\mu_2,-\mu_1;-\lambda_2,-\lambda_1}^{ji}(\theta) , \end{aligned} \quad (5)$$

where the first part comes from (1, 2) alone, while for the last part the CP-invariance relation (4) is also used. On the basis of (5) we could select F_{++++} , F_{++--} , F_{+++-} , F_{+-+-} , F_{+-+-} , F_{+--+} as a possible set of independent helicity amplitudes at each specific angle.

Restricting to real MSSM parameters from here on, it is thus sufficient to only consider the amplitudes of the process $\tilde{\chi}_i^0\tilde{\chi}_j^0 \rightarrow \gamma\gamma$, for both DM and $LC_{\gamma\gamma}$ studies, using the one-loop diagrams generically described in Fig.1, in the 't-Hooft-Feynman gauge. The types of particles running clockwise inside each loop in Fig.1 are: box⁴ (a): ($fSSS$), ($fWWW$), ($fSSW$), ($fSWW$), ($fSWS$), ($fWWS$); box (b): ($Sfff$), ($Wfff$); box (c): ($SffS$), ($WffW$), ($SffW$), ($WffS$); initial triangle⁵ (d): (SfS), (WfW); final triangle⁶ (e): (WWW), (SSS), (SWW), (SSW); final triangle (f): (fff); and bubbles

¹Thus $\lambda_{i,j} = \pm 1/2$ and $\mu_{1,2} = \pm 1$, so that $(-1)^{\mu_1-\mu_2} = 1$.

²These relations do not agree with the antisymmetry condition used in [15].

³We follow the same notation as in *e.g.* [11].

⁴In naming the particle-strings in the box-loop, we always start (moving clockwise) from the line ending to the $\tilde{\chi}_j^0$ vertex.

⁵In naming these particle-strings in Fig.1d, we always start from the line ending to the $\tilde{\chi}_i^0$ -vertex.

⁶The particle-string names in Fig.1e,f, always start from the line leaving the vertex where the s-channel exchanged neutral particle Z , h^0 , H^0 , A^0 or G^0 ends.

(g): (SS) , (WW) ; (h): (WS) . By S we denote the scalar exchanges (Higgs, Goldstone and sfermions); and by f the fermionic ones (leptons, quarks and inos). Bubbles (g) and final triangles (e) and (f), are connected to the initial $\tilde{\chi}_i^0 \tilde{\chi}_j^0$ state through an intermediate Z , or neutral Higgs or Goldstone boson h^0, H^0, A^0, G^0 .

For book-keeping the Majorana nature of the neutralinos, we always describe $\tilde{\chi}_i^0$ by a positive energy Dirac wavefunction, and $\tilde{\chi}_j^0$ by a negative energy one. We then note that the triangle and bubble diagrams in Fig.1, separately satisfy the neutralino and photon symmetry conditions (1, 2). For the separate box-diagrams in Fig.1 though, the photon exchange symmetry is only satisfied after adding to each box of Fig.1, the corresponding photon exchanged one. The calculation of these later boxes may be avoided though, by imposing (2) to the contribution of each of the boxes in Fig.1. Requiring then the validity of (1) for each such box contribution, provides a stringent test of the computation. We have checked that all these constraints are exactly satisfied.

We have derived explicit analytic expressions for the contributions of the various diagrams of Fig.1 in terms of Passarino-Veltman functions [16]. These expressions are so lengthy though, that it is useless to present them explicitly. We have therefore instead chosen to release a numerical code, which calculates the differential cross sections defined below, for various photon polarizations in any MSSM model with real parameters at the electroweak scale; see discussion below.

Before turning to this though, we add two remarks concerning the behavior of the amplitudes near threshold, and at very high energies and angles, respectively. Very close to threshold, the relative orbital angular momentum of the neutralino pair $\tilde{\chi}_i^0 \tilde{\chi}_j^0$ is, of course, vanishing. Because of Fermi statistics, if $i = j$, the neutralino-pair can only exist in an 1S_0 -state corresponding to a total neutralino spin $S_{\text{tot}} = 0$; while if $i \neq j$, $S_{\text{tot}} = 1$ is also possible. In both cases, the CP eigenvalues of the $\tilde{\chi}_i^0 \tilde{\chi}_j^0$ -pair is

$$CP = -(-1)^{S_{\text{tot}}} \eta_i \eta_j \quad .$$

If $S_{\text{tot}} = 0$, then depending on whether $\eta_i \eta_j = 1$ ($\eta_i \eta_j = -1$) the neutralino pair has the same quantum numbers as the A^0 (H^0) neutral Higgs-state, leading to a resonance enhancement for the $\lambda_i = \lambda_j$ -amplitude, whenever the appropriate neutral Higgs mass is close to the sum of the neutralino masses⁷. This is induced by the diagrams in Figs.1e,f,g,h.

Next, concerning the behavior at very high energy ($s \sim |t| \sim |u| \gg M_{\text{SUSY}}\text{-scale}^8$), the dominant leading-log contribution to the neutralino production amplitude is found to be generated by the diagrams in Figs.1a,b,c,d when the internal loops involve chargino and W -exchanges. This is given by

$$F_{\lambda_1 \lambda_2; \mu_1 \mu_2}^{ij} = \tilde{F}_{\mu_1 \mu_2; \lambda_1 \lambda_2}^{ij} \simeq -\frac{\alpha^4}{2s_W^2} \sin \theta \left[C_R \frac{1 + \eta_i \eta_j}{2} \mathbf{L}_R + C_I \frac{1 - \eta_i \eta_j}{2} \mathbf{L}_I \right] + \dots \quad , \quad (6)$$

⁷Since the neutralino masses are heavier than the Z -mass in all contemplated MSSM models, there can never be an analogous enhancement due to the intermediate Z boson in the $i \neq j$, $S_{\text{tot}} = 1$ case.

⁸For such kinematical situations: $t \sim -s(1 - \cos \theta)/2$ and $u \sim -s(1 + \cos \theta)/2$.

where the dots stand for subleading constant and $1/s$ -terms, while

$$\begin{aligned} \mathbb{L}_R &= \left[(\mu_2 - \mu_1)(\lambda_1 - \lambda_2)^2 + 2\mu_1\mu_2(\lambda_1 - \lambda_2)\cos\theta \right] \left[\frac{s}{u} \left(\ln^2 \frac{|t|}{m_W^2} - \ln^2 \frac{s}{m_W^2} + 2i\pi \ln \frac{s}{m_W^2} \right) \right. \\ &+ \left. \frac{s}{t} \left(\ln^2 \frac{|u|}{m_W^2} - \ln^2 \frac{s}{m_W^2} + 2i\pi \ln \frac{s}{m_W^2} \right) \right] + (1 + \mu_1\mu_2)(\lambda_1 - \lambda_2) \left[\frac{s}{u} \left(\ln^2 \frac{|t|}{m_W^2} - \ln^2 \frac{s}{m_W^2} \right. \right. \\ &+ \left. \left. 2i\pi \ln \frac{s}{m_W^2} \right) + \frac{s}{t} \left(\ln^2 \frac{s}{m_W^2} - 2i\pi \ln \frac{s}{m_W^2} - \ln^2 \frac{|u|}{m_W^2} \right) + 2 \left(\ln^2 \frac{|t|}{m_W^2} - \ln^2 \frac{|u|}{m_W^2} \right) \right], \quad (7) \end{aligned}$$

$$\begin{aligned} \mathbb{L}_I &= \left[(\mu_2 - \mu_1)(\lambda_1 - \lambda_2) + 2\mu_1\mu_2(\lambda_1 - \lambda_2)^2 \cos\theta \right] \left[\frac{s}{u} \left(\ln^2 \frac{|t|}{m_W^2} - \ln^2 \frac{s}{m_W^2} + 2i\pi \ln \frac{s}{m_W^2} \right) \right. \\ &+ \left. \frac{s}{t} \left(\ln^2 \frac{|u|}{m_W^2} - \ln^2 \frac{s}{m_W^2} + 2i\pi \ln \frac{s}{m_W^2} \right) \right] + (1 + \mu_1\mu_2)(\lambda_1 - \lambda_2)^2 \left[\frac{s}{u} \left(\ln^2 \frac{|t|}{m_W^2} - \ln^2 \frac{s}{m_W^2} \right. \right. \\ &+ \left. \left. 2i\pi \ln \frac{s}{m_W^2} \right) + \frac{s}{t} \left(\ln^2 \frac{s}{m_W^2} - 2i\pi \ln \frac{s}{m_W^2} - \ln^2 \frac{|u|}{m_W^2} \right) + 2 \left(\ln^2 \frac{|t|}{m_W^2} - \ln^2 \frac{|u|}{m_W^2} \right) \right], \quad (8) \end{aligned}$$

and

$$\begin{aligned} C_R &= 2\text{Re}(Z_{2j}^N Z_{2i}^{N*}) + \frac{1}{2}\text{Re}(Z_{4j}^N Z_{4i}^{N*} + Z_{3j}^N Z_{3i}^{N*}), \\ C_I &= 2i\text{Im}(Z_{2j}^N Z_{2i}^{N*}) + \frac{i}{2}\text{Im}(Z_{4j}^N Z_{4i}^{N*} + Z_{3j}^N Z_{3i}^{N*}), \end{aligned} \quad (9)$$

with $Z_{\alpha j}^N$ describing the neutralino mixing matrix in the notation of [17]. As expected from [18], gauge invariance eliminates all isolated single-log and log-squared terms in (6, 7, 8), so that the only allowed leading-log contribution consists in differences of log-squared terms, i.e. a single $\ln(s/m_W^2)$ multiplied by angular dependent but energy independent logarithmic coefficients for the real part of the amplitudes, and simple $\pi \ln(s/m_W^2)$ -terms for the imaginary parts. At large angles, this has the tendency to enhance the imaginary parts of the amplitudes, as compared to the real parts. Such an asymptotic behavior has also been observed (occasionally very strikingly), for the helicity amplitudes of process like $\gamma\gamma \rightarrow \gamma\gamma$, $Z\gamma$, ZZ , $A^0 A^0$, always being generated by W -loops [13, 19].

Note (from the above expressions of \mathbb{L}_R and \mathbb{L}_I) that, in the high energy limit (when masses are neglected and $s + t + u = 0$) the only non vanishing helicity amplitudes are those with $\lambda_1 = -\lambda_2$ and $\mu_1 = -\mu_2$, i.e. F_{+-+} and F_{+-+} and the ones related by symmetry relations eq.(1-5). This is due to the dominance of box diagrams with chirality conserving gauge couplings of W bosons.

In practice these asymptotic expressions have some interest only when the energy is sufficiently higher than the SUSY scale; for example in the TeV range if the SUSY masses are of the order of a few hundred GeV. At lower energies, two types of effects modify the asymptotic behavior. One is purely kinematic and due to the additional constant and energy decreasing (M^2/s) terms denoted by the dots in (6). The other one is the appearance of chirality violating amplitudes due to box and triangle diagrams involving scalar couplings (neutralino-sfermion-fermion and neutralino-neutralino-Higgs couplings). These amplitudes vanish like M^2/s at high energies, but at energies not too far from

the SUSY scale, their relative importance, compared to the one of the leading chirality conserving ones, is model-dependent. In particular, it depends on the neutralino contents (Bino, Wino and Higgsino mixture) which controls the relative magnitude of its gauge and scalar couplings.

All these properties can be checked by making a numerical comparison with the complete results. We come back to the discussion of these in the next section, where we discuss our results for various benchmark models.

We next turn to the $\gamma\gamma \rightarrow \tilde{\chi}_i^0 \tilde{\chi}_j^0$ collisions in a $\gamma\gamma$ collider $LC_{\gamma\gamma}$ [12] realized through backscattering of laser photons in an e^-e^+ LC [9]. For real MSSM parameters, where CP-invariance holds, the general form of the neutralino production cross section is [13]:

$$\begin{aligned} \frac{d\sigma(\gamma\gamma \rightarrow \tilde{\chi}_i^0 \tilde{\chi}_j^0)}{d\tau d\cos\theta} = & \frac{d\bar{L}_{\gamma\gamma}}{d\tau} \left\{ \frac{d\sigma_0}{d\cos\theta} + \langle \xi_2 \xi'_2 \rangle \frac{d\sigma_{22}}{d\cos\theta} \right. \\ & + \langle \xi_3 \rangle \frac{d\sigma_3}{d\cos\theta} \cos 2\phi + \langle \xi'_3 \rangle \frac{d\sigma'_3}{d\cos\theta} \cos 2\phi' \\ & + \langle \xi_3 \xi'_3 \rangle \left[\frac{d\sigma_{33}}{d\cos\theta} \cos(2[\phi + \phi']) + \frac{d\sigma'_{33}}{d\cos\theta^*} \cos(2[\phi - \phi']) \right] \\ & \left. + \langle \xi_3 \xi'_2 \rangle \frac{d\sigma_{23}}{d\cos\theta} \sin 2\phi + \langle \xi_2 \xi'_3 \rangle \frac{d\sigma'_{23}}{d\cos\theta} \sin 2\phi' \right\} . \end{aligned} \quad (10)$$

In (10), $\tau = s/s_{ee}$, with s_{ee} being the square of the e^-e^+ center-of-mass energy and $s \equiv s_{\gamma\gamma} = s_{\tilde{\chi}_i^0 \tilde{\chi}_j^0}$ denoting the corresponding quantity for the produced neutralino pair. The quantity $d\bar{L}_{\gamma\gamma}/d\tau$ describes the photon-photon luminosity per unit e^-e^+ flux, while the parameter-pairs (ξ_2, ξ'_2) , (ξ_3, ξ'_3) and (ϕ, ϕ') describe respectively the average helicities, transverse polarizations and azimuthal angles of the two backscattered photons. These are in turn determined by the corresponding quantities of the laser photons, and the e^\pm -polarizations [12, 13].

Finally, the σ_n -quantities in (10) are defined as

$$\begin{aligned} \frac{d\sigma_0}{d\cos\theta} &= \left(\frac{C_{ij}}{128\pi s} \right) \sum_{\lambda_1 \lambda_2} [|\tilde{F}_{++\lambda_1 \lambda_2}|^2 + |\tilde{F}_{--\lambda_1 \lambda_2}|^2 + |\tilde{F}_{+-\lambda_1 \lambda_2}|^2 + |\tilde{F}_{-+\lambda_1 \lambda_2}|^2] , \\ &= \left(\frac{C_{ij}}{64\pi s} \right) [|\tilde{F}_{++++}|^2 + |\tilde{F}_{++--}|^2 + |\tilde{F}_{+++-}|^2 + |\tilde{F}_{++-+}|^2 \\ &\quad + |\tilde{F}_{+-+-}|^2 + |\tilde{F}_{+---}|^2 + |\tilde{F}_{+-+-}|^2 + |\tilde{F}_{+--+}|^2] , \end{aligned} \quad (11)$$

$$\begin{aligned} \frac{d\sigma_{22}}{d\cos\theta} &= \left(\frac{C_{ij}}{128\pi s} \right) \sum_{\lambda_1 \lambda_2} [|\tilde{F}_{++\lambda_1 \lambda_2}|^2 + |\tilde{F}_{--\lambda_1 \lambda_2}|^2 - |\tilde{F}_{+-\lambda_1 \lambda_2}|^2 - |\tilde{F}_{-+\lambda_1 \lambda_2}|^2] \\ &= \left(\frac{C_{ij}}{64\pi s} \right) [|\tilde{F}_{++++}|^2 + |\tilde{F}_{++--}|^2 + |\tilde{F}_{+++-}|^2 + |\tilde{F}_{++-+}|^2 \\ &\quad - (|\tilde{F}_{+-+-}|^2 + |\tilde{F}_{+---}|^2 + |\tilde{F}_{+-+-}|^2 + |\tilde{F}_{+--+}|^2)] , \end{aligned} \quad (12)$$

$$\begin{aligned}
\frac{d\sigma_3}{d\cos\theta} &= \left(\frac{-C_{ij}}{64\pi s}\right) \sum_{\lambda_1\lambda_2} [\tilde{F}_{++\lambda_1\lambda_2}\tilde{F}_{-\lambda_1\lambda_2}^* + \tilde{F}_{+-\lambda_1\lambda_2}\tilde{F}_{-\lambda_1\lambda_2}^*] \\
&= \left(\frac{-C_{ij}}{32\pi s}\right) \text{Re}[\tilde{F}_{++++}\tilde{F}_{----}^* + \tilde{F}_{+--+}\tilde{F}_{-+--}^* \\
&\quad - \tilde{F}_{+++-}\tilde{F}_{+-+-}^* - \tilde{F}_{++-+}\tilde{F}_{+-+-}^*] \eta_i\eta_j , \tag{13}
\end{aligned}$$

$$\begin{aligned}
\frac{d\sigma'_3}{d\cos\theta} &= \left(\frac{-C_{ij}}{64\pi s}\right) \sum_{\lambda_1\lambda_2} [\tilde{F}_{++\lambda_1\lambda_2}\tilde{F}_{-\lambda_1\lambda_2}^* + \tilde{F}_{-\lambda_1\lambda_2}\tilde{F}_{--\lambda_1\lambda_2}^*] \\
&= \left(\frac{-C_{ij}}{32\pi s}\right) \text{Re}[\tilde{F}_{++++}\tilde{F}_{+-++}^* + \tilde{F}_{+--+}\tilde{F}_{----}^* \\
&\quad + \tilde{F}_{+++-}\tilde{F}_{+-+-}^* + \tilde{F}_{++-+}\tilde{F}_{+-+-}^*] , \tag{14}
\end{aligned}$$

$$\begin{aligned}
\frac{d\sigma_{33}}{d\cos\theta} &= \left(\frac{C_{ij}}{32\pi s}\right) \text{Re}[\tilde{F}_{----}\tilde{F}_{-+--}^* + \tilde{F}_{+--+}\tilde{F}_{-+--}^*] \\
&= \left(\frac{C_{ij}}{32\pi s}\right) \text{Re}[\tilde{F}_{----}\tilde{F}_{-+--}^* - \tilde{F}_{+--+}\tilde{F}_{-+--}^*] \eta_i\eta_j , \tag{15}
\end{aligned}$$

$$\begin{aligned}
\frac{d\sigma'_{33}}{d\cos\theta} &= \left(\frac{C_{ij}}{32\pi s}\right) \text{Re}[\tilde{F}_{++++}\tilde{F}_{--++}^* + \tilde{F}_{+++-}\tilde{F}_{--++}^*] \\
&= \left(\frac{C_{ij}}{32\pi s}\right) \text{Re}[\tilde{F}_{++++}\tilde{F}_{++--}^* - \tilde{F}_{+++-}\tilde{F}_{++--}^*] \eta_i\eta_j , \tag{16}
\end{aligned}$$

$$\begin{aligned}
\frac{d\sigma_{23}}{d\cos\theta} &= \left(\frac{-C_{ij}}{32\pi s}\right) \text{Im}[\tilde{F}_{++++}\tilde{F}_{+---}^* + \tilde{F}_{+--+}\tilde{F}_{+---}^* \\
&\quad - \tilde{F}_{+++-}\tilde{F}_{+-+-}^* - \tilde{F}_{++-+}\tilde{F}_{+-+-}^*] \eta_i\eta_j , \tag{17}
\end{aligned}$$

$$\begin{aligned}
\frac{d\sigma'_{23}}{d\cos\theta} &= \left(\frac{C_{ij}}{32\pi s}\right) \text{Im}[\tilde{F}_{++++}\tilde{F}_{+-++}^* + \tilde{F}_{+--+}\tilde{F}_{+-++}^* \\
&\quad + \tilde{F}_{+++-}\tilde{F}_{+-+-}^* + \tilde{F}_{++-+}\tilde{F}_{+-+-}^*] , \tag{18}
\end{aligned}$$

where the reduction due to the identity of the final neutralinos whenever $i = j$, is taken into account through the coefficient

$$\begin{aligned}
C_{ij} &= \beta_{ij} \left(1 - \frac{\delta_{ij}}{2}\right) , \\
\beta_{ij} &= \sqrt{\left[1 - \frac{(m_i - m_j)^2}{s}\right] \left[1 - \frac{(m_i + m_j)^2}{s}\right]} , \tag{19}
\end{aligned}$$

and the c.m. scattering angle θ varies in the range $-1 \leq \cos\theta \leq +1$.

On the basis of (1, 2) we obtain that $d\sigma_0/d\cos\theta$, $d\sigma_{22}/d\cos\theta$, $d\sigma_{33}/d\cos\theta$ and $d\sigma'_{33}/d\cos\theta$ are symmetric under the interchange

$$\theta \leftrightarrow \pi - \theta \quad ,$$

whereas

$$\begin{aligned} \frac{d\sigma_3}{d\cos\theta}|_\theta &= \frac{d\sigma'_3}{d\cos\theta}|_{\pi-\theta} \quad , \\ \frac{d\sigma_{23}}{d\cos\theta}|_\theta &= -\frac{d\sigma'_{23}}{d\cos\theta}|_{\pi-\theta} \quad . \end{aligned}$$

3 Results

On the basis of the diagrams in Fig.1, we have constructed a numerical code called PLATONlc which calculates the differential cross sections in (11-18) for any c.m. energy and any set of real MSSM parameters at the electroweak scale, using [20]. This code, together with an explanatory Readme file, can be downloaded from [21].

We have made a run for the 31 benchmark models already used in the previous DM study in [7]. For each model we have computed both the angular distribution and the energy dependence of the various cross sections presented in Section 2, for $\tilde{\chi}_1^0\tilde{\chi}_1^0$, $\tilde{\chi}_1^0\tilde{\chi}_2^0$ and $\tilde{\chi}_2^0\tilde{\chi}_2^0$ production.

The typical feature of the angular distribution is an isotropy at low energy, and a tendency to present some forward-backward peaking at high energies (see the $1/t$ and $1/u$ terms in eq.(7, 8)). For the integrated cross sections, one finds energy dependent structures at $s \sim (m_1 + m_2)^2$, with $m_{1,2}$ being the masses of intermediate particles contributing to the diagrams of Fig.1, as well as resonance effects due to diagrams involving A^0 or H^0 intermediate neutral Higgs-states.

These features are common to several benchmark models, so we will not illustrate all of them. Moreover, since the expected luminosities at the future colliders will probably be of the order of 10^2 fb^{-1} per year, we ignore those model-cases considered in [7], where the cross sections are much smaller than $\sim 0.1 \text{ fb}$. We thus present results for the universal mSUGRA benchmark models [22] $SPS1a_1$, $SPS4$ [23], $AD(fg5)_1$ [24]; the non-universal mSUGRA models CDG_{75} and CDG_{OII} [25]; and the GMSB models [26] $SPS7_1$, $SPS8_1$ [23]. The grand scale defining parameters for all these cases are shown in Table 1.

Starting from the grand-scale parameters in Table 1, their electroweak scale values and the H^0 and A^0 widths are calculated using the codes SuSpect [27] and HDECAY [28]. In turn, these values constitute the input needed for the PLATONlc code [21]. The obtained results are indicated in Figs.2-8 below. In all cases, the sub-figures labelled (a), (b) and (c) describe the integrated cross sections of Eqs.(11-18), in the range $(1^\circ < \theta < 179^\circ)$ for $\tilde{\chi}_1^0\tilde{\chi}_1^0$, $\tilde{\chi}_1^0\tilde{\chi}_2^0$ and $\tilde{\chi}_2^0\tilde{\chi}_2^0$ production respectively. Of course, only $\tilde{\chi}_1^0\tilde{\chi}_2^0$ and $\tilde{\chi}_2^0\tilde{\chi}_2^0$ production are in principle observable, since the lightest supersymmetric particle LSP $\tilde{\chi}_1^0$ should be invisible in an R-conserving theory. In addition, sub-figures (d) and (e) give the unpolarized

Table 1: Input parameters for the used MSSM benchmark models at the grand scale. Dimensions in GeV. In all cases $\mu > 0$. By convention, $M_2 > 0$ is used.

	universal mSUGRA			non-universal mSUGRA		GMSB		
	<i>SPS1a</i> ₁	<i>AD(fg5)</i> ₁	<i>SPS4</i>	<i>CDG</i> ₇₅	<i>CDG</i> _{OII}		<i>SPS7</i> ₁	<i>SPS8</i> ₁
M_1	250	400	300	-400	424	M_{mess}	80000	120000
M_2	250	400	300	240	200	M_{SUSY}	40000	60000
M_3	250	400	300	80	40	$\tan \beta$	15	15
m_0	100	220	400	1400	1400			
m_{H_u}	100	220	400	1400	1400			
A_0	-100	0	0	1000	1000			
$\tan \beta$	5	40	50	50	50			

differential cross section $d\sigma_0/d\cos\theta$ at c.m energies 0.4 and 2 TeV respectively, for the $\tilde{\chi}_i^0\tilde{\chi}_j^0$ production channels which are energetically accessible. On the basis of Figs.2-8, we remark the following:

In the universal mSUGRA cases of Figs.2-4 and the non-universal mSUGRA CDG_{75} of Fig.5, only the σ_0 , σ_{22} and occasionally the $\sigma_3 = \sigma'_3$ cross sections for $\gamma\gamma \rightarrow \tilde{\chi}_2^0\tilde{\chi}_2^0$, are sufficiently large to be (in principle) observable in a conceivable future Collider. This is because $\tilde{\chi}_2^0 \sim \tilde{W}^{(3)}$ and $\tilde{\chi}_1^0 \sim \tilde{B}$, in these models. The largest and easier to measure cross section is, of course, the unpolarized σ_0 , defined in (11). As seen from Figs.2-5(c) though, in an $LC_{\gamma\gamma}$ collider at 0.4 TeV, the $\tilde{\chi}_2^0\tilde{\chi}_2^0$ -pair production can only occur in the case of the *SPS1a*₁ and *CDG*₇₅ models. In all other cases, $\tilde{\chi}_2^0$ is too heavy to be produced at 0.4 TeV, but it can be generated in a 2TeV $\gamma\gamma$ version of CLIC; compare Figs.2-5(d). As seen there, $d\sigma_0/d\cos\theta$ is very flat at 0.4TeV, and develops a moderate forward-backward peak already at 2TeV.

Fig.6 concerns the *OII* non-universal mSUGRA model of [25], where $\tilde{\chi}_1^0$ is predominantly a Wino with some appreciable Higgsino components, while $\tilde{\chi}_2^0$ is predominantly a Bino. Depending on the $LC_{\gamma\gamma}$ energy and flux, both $\tilde{\chi}_1^0\tilde{\chi}_2^0$ and $\tilde{\chi}_2^0\tilde{\chi}_2^0$ productions may be observable. A special feature of this model is that $\tilde{\chi}_1^0\tilde{\chi}_2^0$ production is predicted to be generally more copious than the $\tilde{\chi}_2^0\tilde{\chi}_2^0$ one. Although, $d\sigma_0/d\cos\theta$ is very flat at 0.4TeV for all channels, it develops strong forward-backward peaks by the time the energy reaches 2TeV; compare subfigures (c) and (d).

Concerning the GMSB models [26] in Figs.7,8, we remark that their general structure is reminiscent of the results in the mSUGRA models of Figs.2-4. Finally, no results are presented for the AMSB models [29, 23], since the almost exact relations $\tilde{\chi}_1^0 \sim \tilde{W}$ and $\tilde{\chi}_2^0 \sim \tilde{B}$ there, enforce unobservably small values for the $\tilde{\chi}_1^0\tilde{\chi}_2^0$ and $\tilde{\chi}_2^0\tilde{\chi}_2^0$ production cross sections.

We next turn to the comparison of the numerical results from the exact 1-loop computations, with those from the asymptotic expressions in (6,7, 8). First, we observed that in all benchmark models considered above, the chirality violating amplitude F_{++++} , and the

chirality conserving F_{+-+} and F_{+--} , are the dominant ones at energies above 1 TeV. In all cases, F_{++++} is strongly decreasing with energy in the several TeV range; while F_{-+-} and F_{+--} become increasingly dominant (with increasing energy) approaching their asymptotic expressions from (6), up to a constant. Since (6) is generated by chargino-W loops, the accuracy of the asymptotic expressions at high energies is particularly striking for cases where the produced neutralino is mainly a Wino. A best example of these is illustrated in Fig.9 for $\tilde{\chi}_2 \tilde{\chi}_2$ production in the $AD(fg5)_1$ model. There exist cases though, particularly in the production of Bino-like neutralinos, where the constant departure between exact and asymptotic expressions for the F_{+-+} and F_{+--} amplitudes, and the subleading F_{++++} amplitude, are still important at the few TeV energy region.

In practice it means that an amplitude analysis of experimental data at high energy could immediately determine the nature of the produced neutralinos. If a precise amplitude analysis is not possible, at least a fit of the unpolarized cross section of the type $a + b \ln(s/m_W^2) + c \ln^2(s/m_W^2)$ should produce a measurement of the logarithmic slope c , which could then be compared to the model predictions for the square of the quantities C_R or C_I in (9), thereby providing clean tests of the neutralino properties.

4 Conclusions

In this paper we have presented our work on the properties of the process $\gamma\gamma \rightarrow \tilde{\chi}_i^0 \tilde{\chi}_j^0$, that are measurable in a $\gamma\gamma$ linear collider $LC_{\gamma\gamma}$. It complements the study of the reverse process in [7], which was adjusted to the environment of the Dark Matter searches. In both cases, the complete set of Feynman diagrams has been calculated.

As in [7], we have found that these processes are very sensitive to the actual values of the various MSSM parameters, and details of the neutralino mixings in particular. The basic size of the cross sections can vary by several orders of magnitude, depending on the contents of the produced neutralinos, the highest values being obtained when neutralinos are Wino-like. Depending on the SUSY model, these properties reflect in a variable way in the $\tilde{\chi}_1^0 \tilde{\chi}_2^0$ and $\tilde{\chi}_2^0 \tilde{\chi}_2^0$ productions. Further enhancements can appear locally owing to the occurrence of threshold effects due to relatively light intermediate states in box diagrams or of A^0 , H^0 resonance effects.

In the low and medium energy range these processes depend on most of the MSSM parameters (because of the variety of particles appearing as intermediate states in the one loop diagrams of Fig.1) but we have also shown that, in the high energy limit, the amplitudes tend to a simple logarithmic form with a coefficient that only depends on the neutralino mixing matrices Z^N without any other SUSY parameter.

The angular distribution of the differential cross sections is generally rather flat at low energy, but a simple forward-backward peaking is progressively generated according with the asymptotic rule mentioned above.

These processes have a very rich supersymmetric contents (in fact all SUSY particles, except gluinos, contribute) so that measurements at variable energy should provide very

stringent tests of MSSM and the neutralino structure.

Concerning in particular the Linear Collider measurements, we should remember that the $LC_{\gamma\gamma}$ study of the $\gamma\gamma \rightarrow \tilde{\chi}_i^0 \tilde{\chi}_j^0$ -process, complements the study of the tree level LC observables for $e^- e^+ \rightarrow \tilde{\chi}_i^0 \tilde{\chi}_j^0$. If MSSM is really valid, and neutralinos turn out to be accessible to future LC and $LC_{\gamma\gamma}$, the combined analyses of such experiments can increase our knowledge on the nature of neutralinos and of SUSY in general.

But the most important fact is that they can be combined with the dark matter searches, thus allowing exchange of knowledge between accelerator particle physics and astrophysics. To facilitate future work on LC or DM studies, the numerical codes PLATONlc and PLATONDml have been released, calculating the Linear Collider differential cross sections and the Dark Matter rates respectively [21]. These codes are applicable to any MSSM model with real parameters at the electroweak scale⁹.

Acknowledgments:

It is a pleasure to thank Abdelhak Djouadi and Jean-Loïc Kneur for very helpful discussions.

⁹By convention we always select $M_2 > 0$.

References

- [1] D.N. Spergel *et.al.* arXiv:astro-ph/0302209.
- [2] G. Jungman, M. Kamionkowski and K. Griest, Phys. Rep. **267**:195 (1996); M. Kamionkowski, hep-ph/0210370.
- [3] M. Drees, Pramana **51**,87(1998); M.S. Turner, J.A. Tyson, astro-ph/9901113, Rev. Mod. Phys. **71S**:145(1999); M.M. Nojiri, hep-ph/0305192; M. Drees hep-ph/0210142; J. Ellis, astro-ph/0304183.
- [4] L. Bergström and P. Ullio, Nucl. Phys. **B504**:27 (1997).
- [5] Z. Bern, P. Gondolo and M. Perelstein, Phys. Lett. **B411**:86 (1997).
- [6] P. Ullio and L. Bergström Phys. Rev. **D57**:1962 (1998).
- [7] G.J. Gounaris, J. Layssac, P.I. Porfyriadis, F.M. Renard, arXiv:hep-ph/0309032.
- [8] D.S. Akerib, S.M. Carroll, M. Kamionkowski and S. Ritz, hep-ph/0201178.
- [9] J.A. Aguilar-Saavedra *et.al.*, TESLA-report SLAC-reprint-2001-002, (Mar 2001), arXiv:hep-ph/0106315; E. Accomando *et.al.* , Phys. Rev. **299**:1 (1998), arXiv:hep-ph/9705442.
- [10] A. Bartl, H. Fraas and W. Majerotto, Nucl. Phys. **B278**:1 (186); S.Y. Choi, A. Djouadi, M. Guchait, J. Kalinowski, H.S. Song and P.M. Zerwas, Eur. Phys. J. **C14**:535 (2000); G. Moortgat-Pick, A. Bartl, H. Fraas and W. Majerotto arXiv:hep-ph/0002253, arXiv:hep-ph/0007222; A. Bartl, T. Kernreiter and O. Kittel, arXiv:hep-ph/0309340.
- [11] G.J. Gounaris, C. Le Mouël and P.I. Porfyriadis Phys. Rev. **D65**:035002 (2002); G.J. Gounaris and C. Le Mouël Phys. Rev. **D66**:055007 (2002).
- [12] I.F. Ginzburg, G.L. Kotkin, V.G. Serbo and V.I. Telnov, Nucl. Instr. and Meth. **205**:47 (1983); I.F. Ginzburg, G.L. Kotkin, V.G. Serbo, S.L. Panfil and V.I. Telnov, Nucl. Instr. and Meth. **219**:5 (1984); J.H. Kühn, E. Mirkes and J. Steegborn, Z. f. Phys. **C57**:615 (1993); R. Brinkman *et.al.* hep-ex/9707017; V. Telnov hep-ex/9802003, hep-ex/9805002.
- [13] G.J. Gounaris, P.I. Porfyriadis and F.M. Renard Eur. Phys. J. **C9**:673 (1999), arXiv:hep-ph/9902230; G.J. Gounaris, J. Layssac, P.I. Porfyriadis and F.M. Renard Eur. Phys. J. **C10**:499 (1999), arXiv:hep-ph/9904450; G.J. Gounaris, J. Layssac, P.I. Porfyriadis and F.M. Renard Eur. Phys. J. **C13**:79 (2000), arXiv:hep-ph/9909243; G.J. Gounaris, P.I. Porfyriadis and F.M. Renard Eur. Phys. J. **C19**:57 (2001), arXiv:hep-ph/0010006.
- [14] M. Jacob and G.C. Wick, Annals of Phys. **7**:404 (1959).

- [15] Zhou Fei, Ma Wen-Gam, Jiang Yi and Han Liang, Phys. Rev. **D62**:115006 (2000).
- [16] G. Passarino and M. Veltman, Nucl. Phys. **B160**:151 (1979).
- [17] J. Rosiek, Phys. Rev. **D41**:3464 (1990), hep-ph/9511250(E).
- [18] M. Beccaria, P. Ciafaloni, D. Comeli, F.M. Renard and C. Verzegnassi, Phys. Rev. **D61**:073005 (2000); ibid Phys. Rev. **D61**:011301 (2000); A. Denner and S. Pozzorini Eur. Phys. J. **C18**:461 (2001); ibid Eur. Phys. J. **C21**:63 (2001); M. Beccaria, F.M. Renard and C. Verzegnassi, Phys. Rev. **D63**:095010 (2001); ibid Phys. Rev. **D63**:043013 (2001); M. Beccaria, M. Melles, F.M. Renard and C. Verzegnassi, Phys. Rev. **D65**:093007 (2002); M. Beccaria, M. Melles, F.M. Renard, S. Trimarchi and C. Verzegnassi, arXiv:hep-ph/0304110.
- [19] G.J. Gounaris, P.I. Porfyriadis Eur. Phys. J. **C18**:181 (2000).
- [20] G.J. van Oldenborgh and J.A. Vermaseren, Z. f. Phys. **C46**:425 (1990); T. Hahn and M. P/erez-Victoria, Comput. Phys. Commun. **118**:153 (1999); T. Hahn *Loop Tools 2 User's Guide* (2001) [[http://www.feynarts/de/looptools](http://www.feynarts.de/looptools)].
- [21] PLATON codes can be downloaded from <http://dtp.physics.auth.gr/platon/>
- [22] A.H. Chamseddine, R. Arnowitt and P. Nath, Phys. Rev. Lett. **49**:970 (1982); R. Barbieri, S. Ferrara and C.A. Savoy, Phys. Lett. **B119**:343 (1982); L. Hall, J. Lykken and S. Weinberg Phys. Rev. **D27**:2359 (1983).
- [23] B.C. Allanach et al, Eur. Phys. J. **C25**:113 (2002), hep-ph/0202233; G. Weiglein, hep-ph/0301111.
- [24] R. Arnowitt and B. Dutta, talk at 10th Int. Conf. on Supersymmetry and Unification of Fundamental Interactions (SUSY02), Hamburg, 2002 (hep-ph/0211042).
- [25] C.H. Chen, M. Drees and J.F. Gunion, Phys. Rev. **D55**:330 (1997) and (E) Phys. Rev. **D60**:039901 (1999); J. Amundson *et.al.* , Report of the Snowmass Supersymmetry Theory Working Group, hep-ph/9609374; A. Djouadi, Y. Mambrini and M. Mühlleitner, hep-ph/0104115, Eur. Phys. J. **C20**:563 (2001).
- [26] M. Dine and A.E. Nelson, Phys. Rev. **D48**:1277 (1993); M. Dine, A.E. Nelson and Y. Shirman Phys. Rev. **D51**:1362 (1995); M. Dine, A.E. Nelson, Y. Nir and Y. Shirman Phys. Rev. **D53**:2658 (1996); N. Arkani-Hamed, J. March-Russel and H. Murayama, Nucl. Phys. **B509**:3 (1998); H. Murayama Phys. Rev. Lett. **79**:18 (1997); K.I. Izawa, Y. Nomura, K. Tobe and T. Yanagida, Phys. Rev. **D56**:2886 (1997); M.A. Luty Phys. Lett. **B414**:71 (1997).
- [27] "SuSpect", A. Djouadi, J.-L. Kneur and G. Moultaka, hep-ph/0211331,
- [28] "HDECAY", A. Djouadi, J. Kalinowski and M. Spira, Comput. Phys. Commun. **108**:56 (1998); <http://www.desy.de/~spira/hdecay>.

[29] L. Randall and R. Sundrum, Nucl. Phys. **B557**:79 (1999); G. Giudice, M. Luty, H. Murayama and R. Rattazzi, JHEP **9812**:027 (1998); J.A. Bagger, T. Moroi and E. Poppitz, JHEP **0004**:009 (2000).

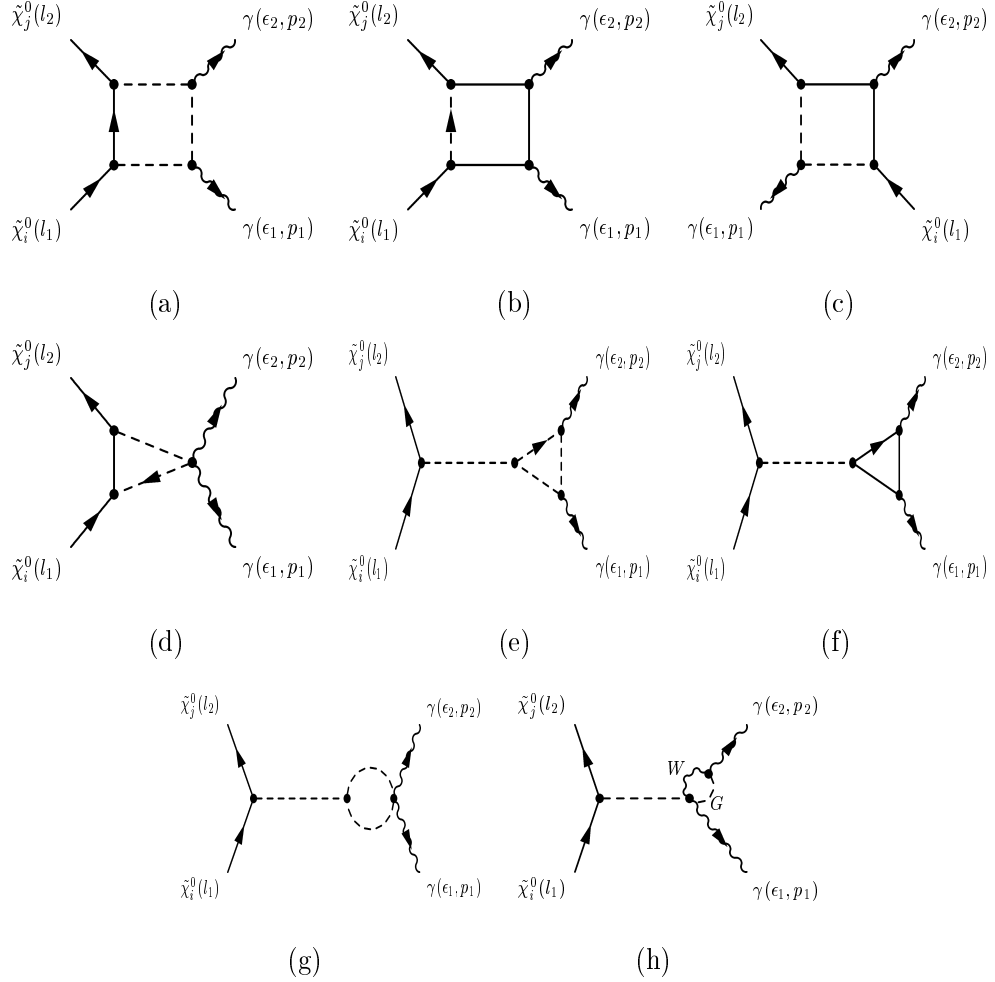


Figure 1: Feynman diagrams for $\tilde{\chi}_i^0 \tilde{\chi}_j^0 \rightarrow \gamma\gamma$. Full internal lines denote fermionic exchanges; while broken internal lines denote either scalar or gauge exchanges, except in the diagram (h), where the W and Goldstone exchanges are indicated explicitly.

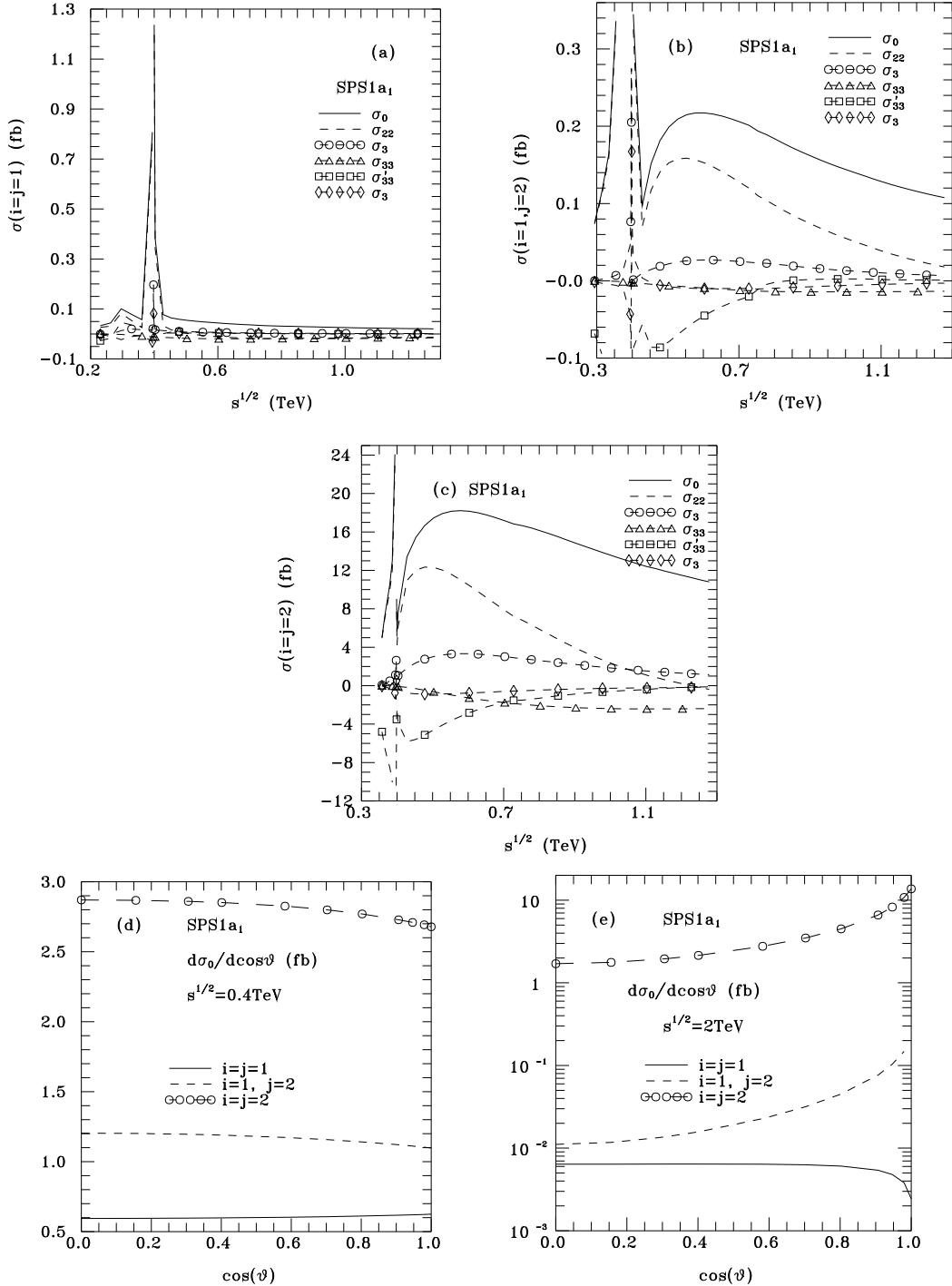


Figure 2: The integrated cross sections for $\gamma\gamma \rightarrow \tilde{\chi}_i^0 \tilde{\chi}_j^0$ in the benchmark model $SPS1a_1$ [23] at a variable energy: $i=1 j=1$ (a), $i=1 j=2$ (b), $i=2 j=2$ (c). The angular distributions for σ_0 in the same model are given at 0.4 TeV (d) and 2 TeV (e). In all cases $\alpha = 1/137$ is used.

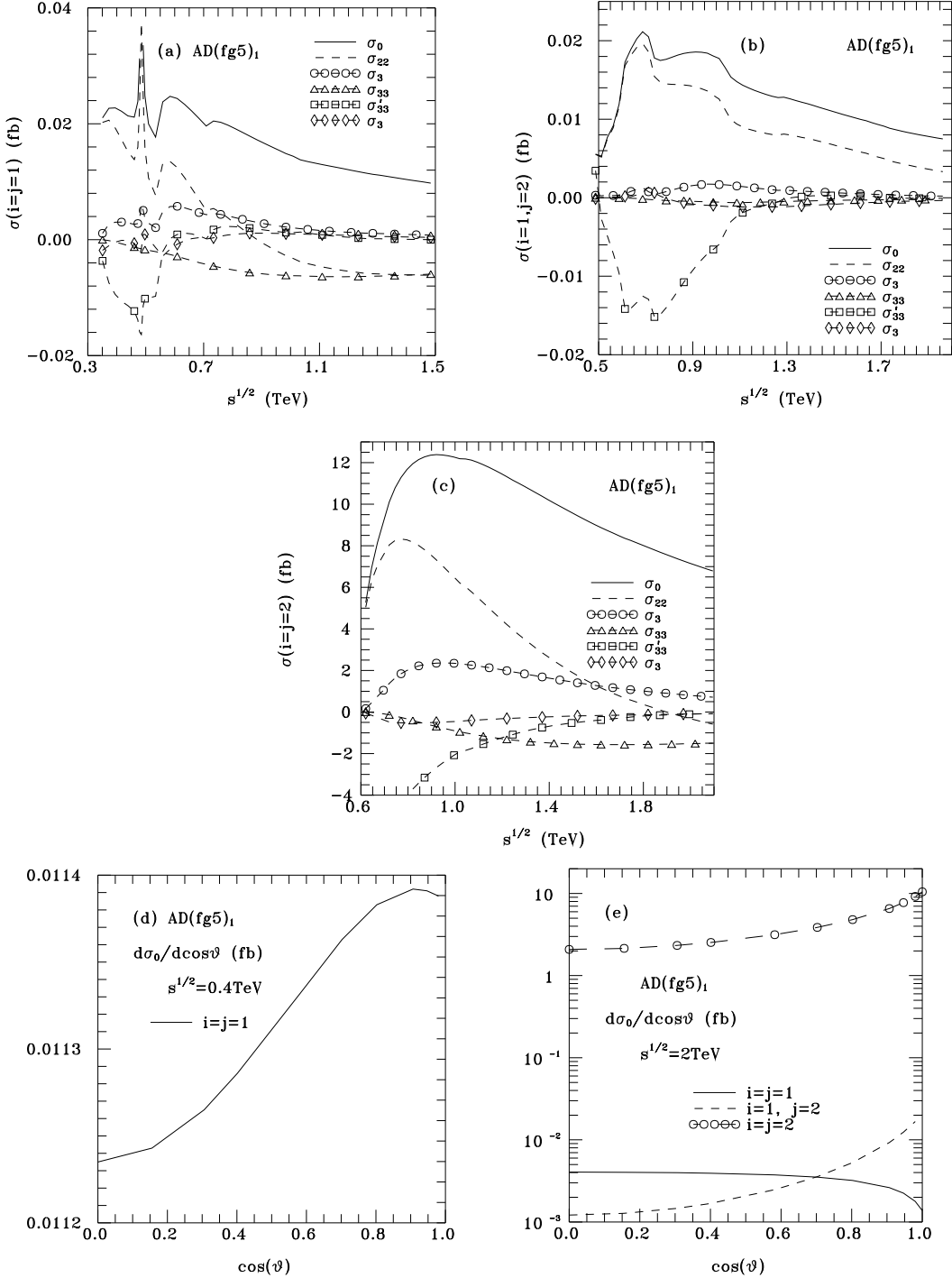


Figure 3: Same caption as in Fig.2 for the benchmark model $AD(fg5)_1$ [24].

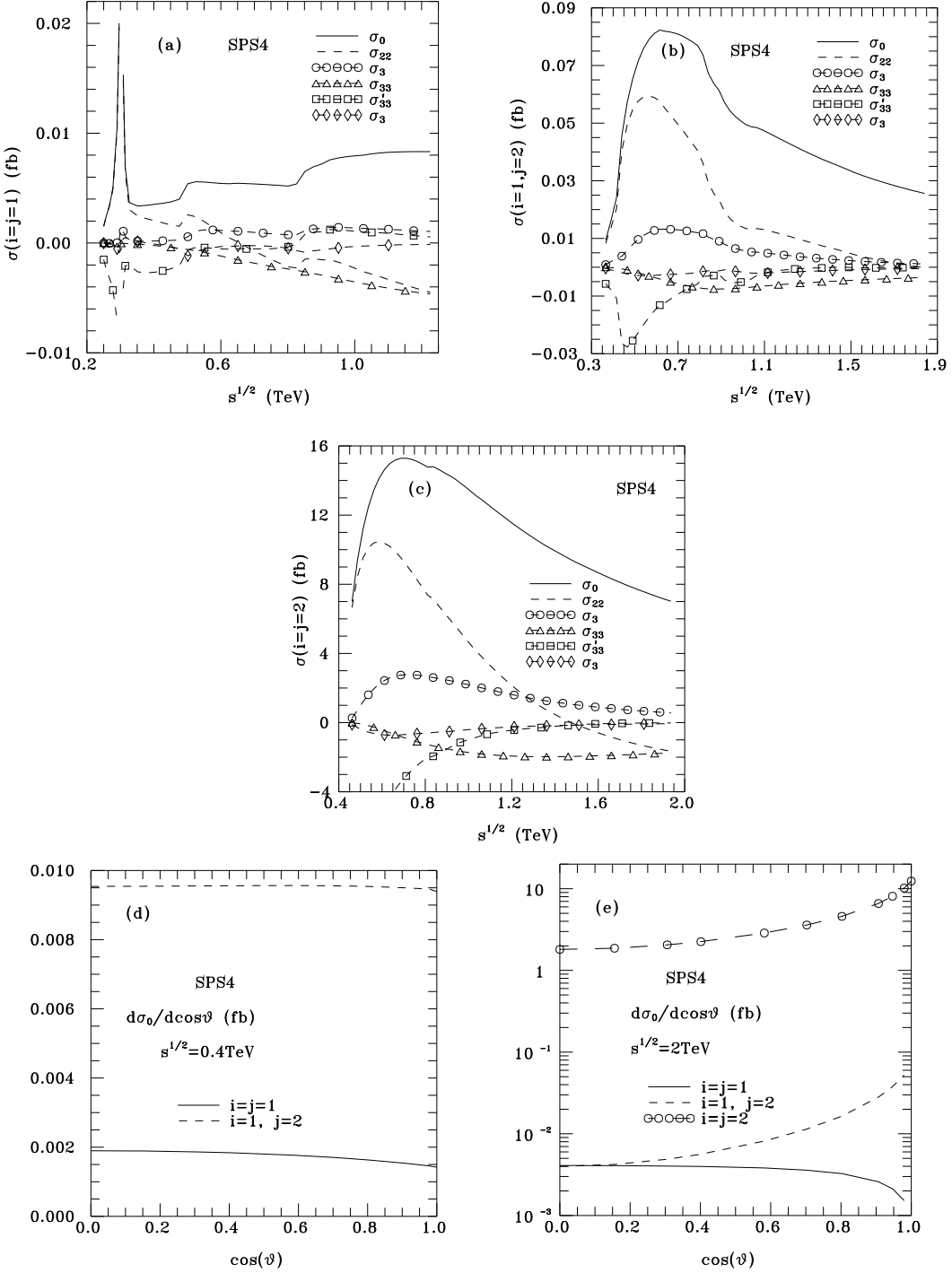


Figure 4: Same caption as in Fig.2 for the benchmark model *SPS4* [23].

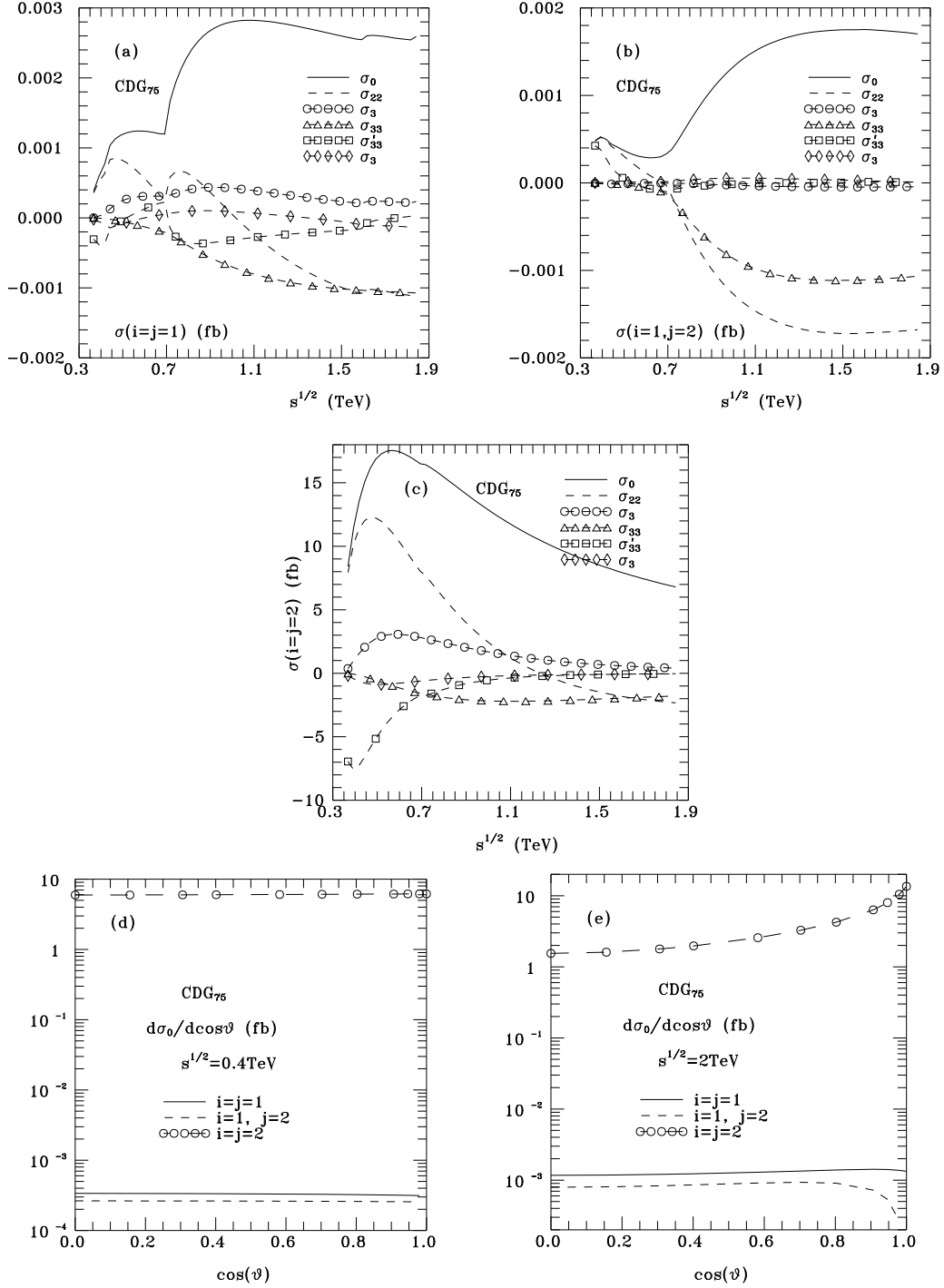


Figure 5: Same caption as in Fig.2 for the benchmark model CDG_{75} [25].

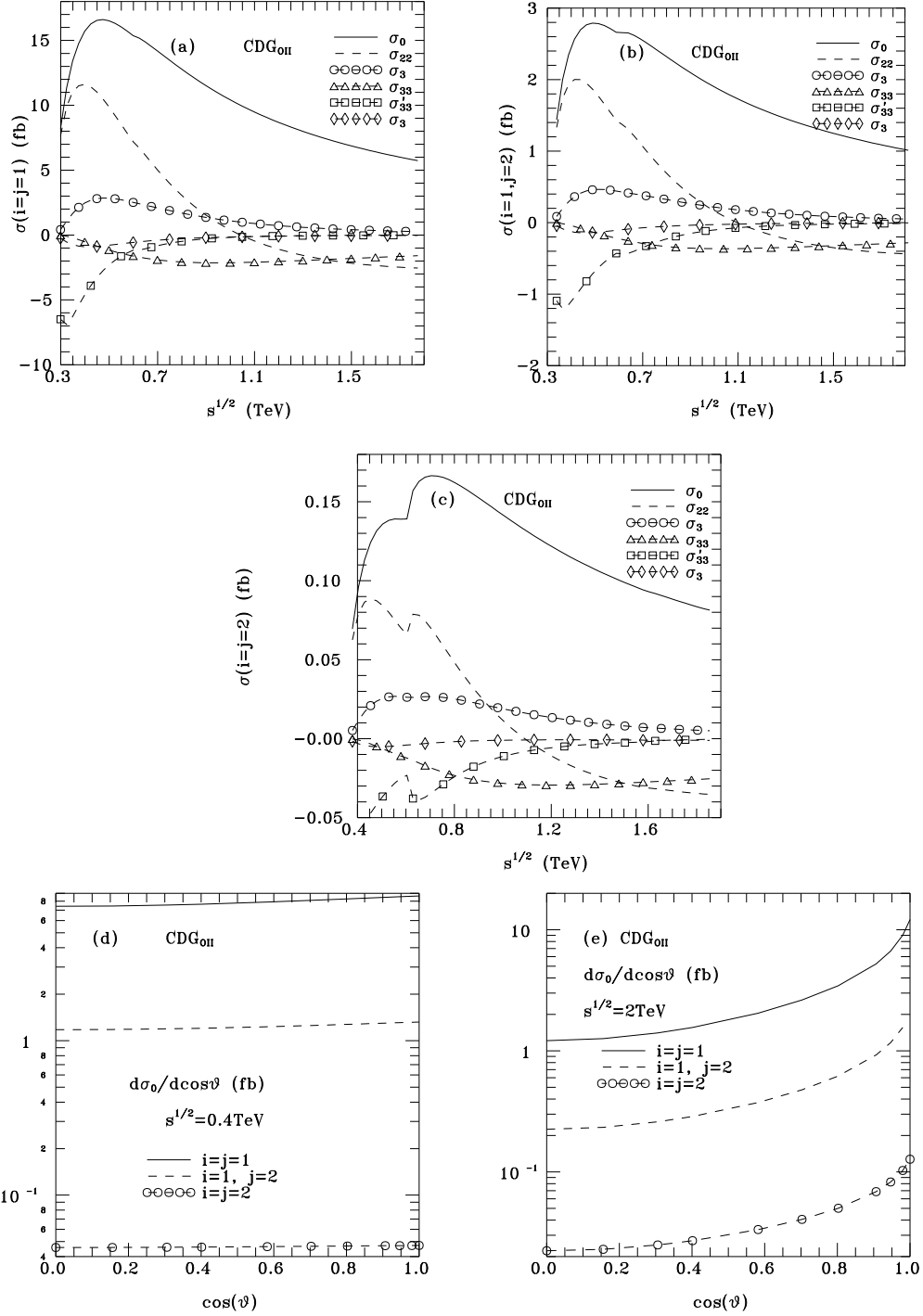


Figure 6: Same caption as in Fig.2 for the benchmark model CDG_{OII} [25].

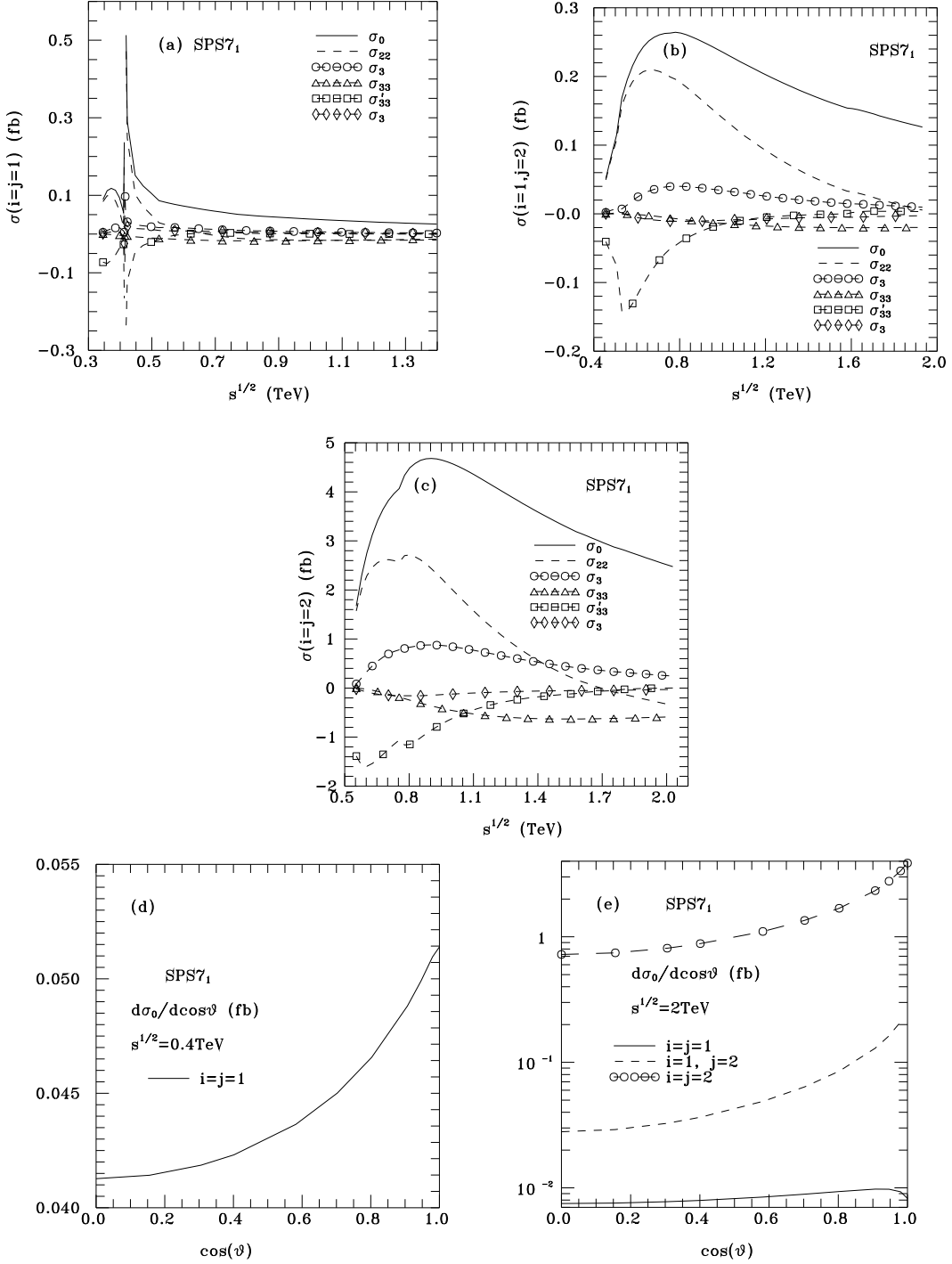


Figure 7: Same caption as in Fig.2 for the benchmark model *SPS7₁* [23].

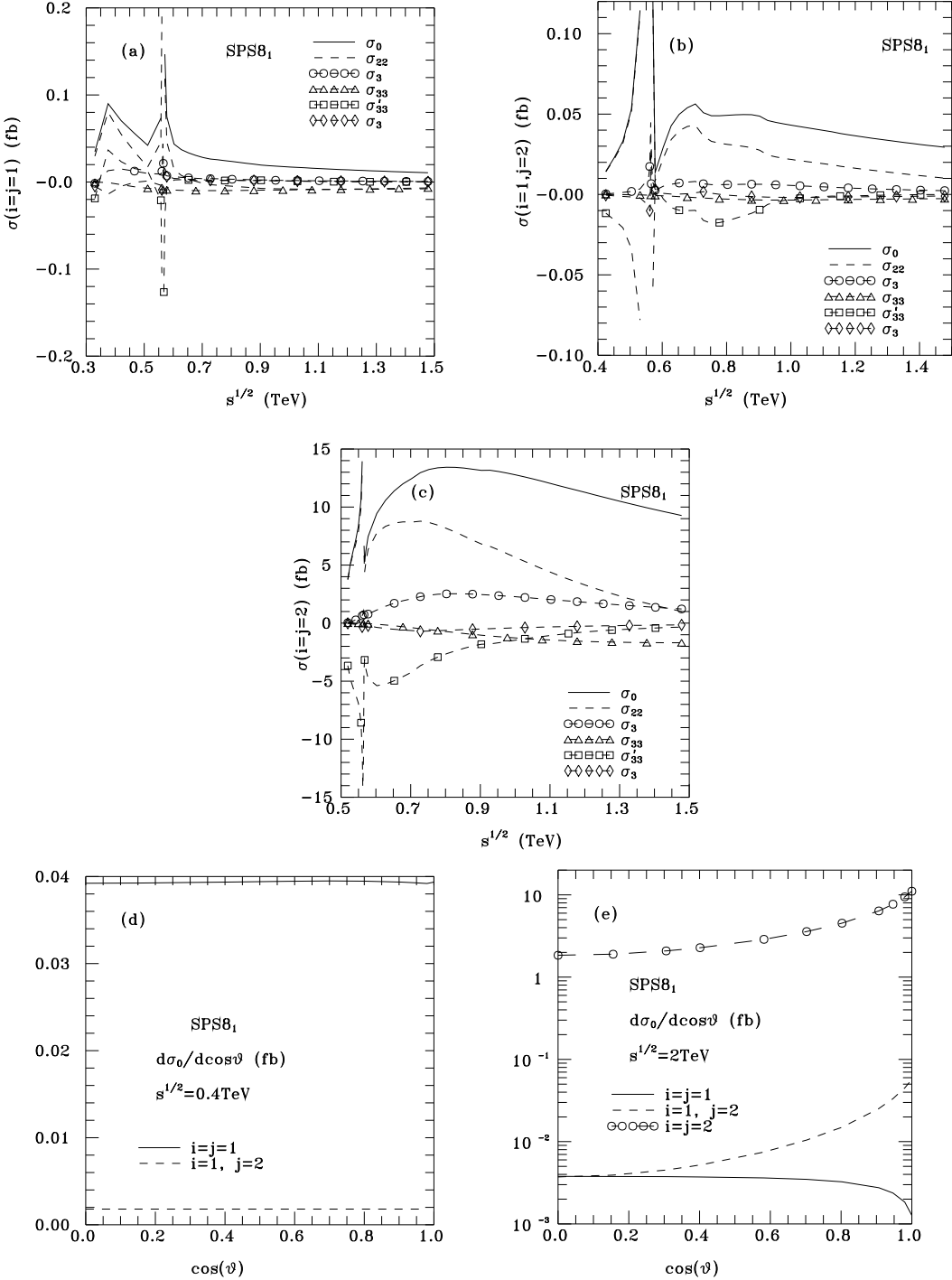


Figure 8: Same caption as in Fig.2 for the benchmark model $SPS8_1$ [23].

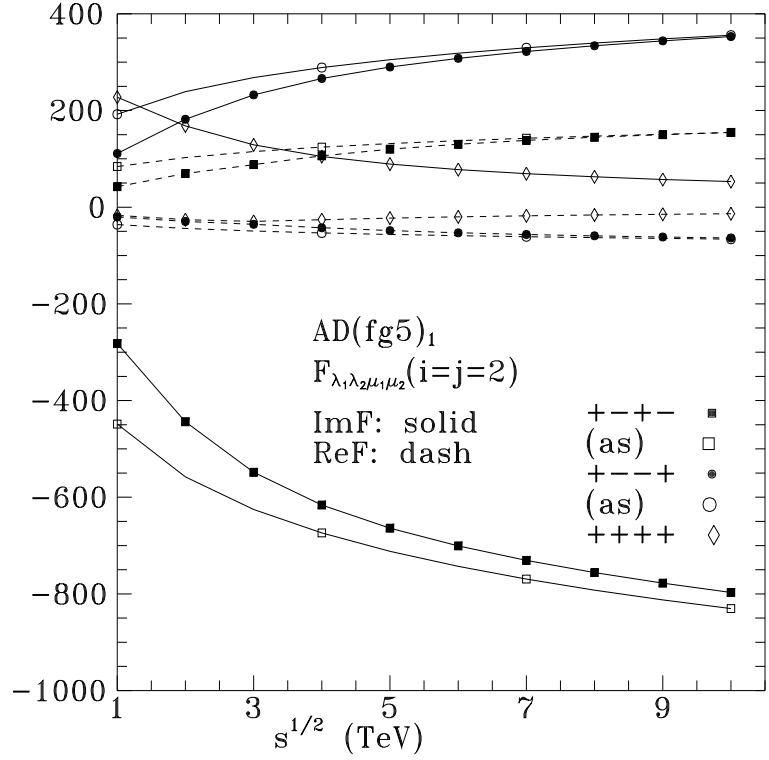


Figure 9: The exact and asymptotic (indicated by "as") 1-loop expressions for the real and imaginary parts of the F_{+-+} , F_{+--} and F_{+++} helicity amplitudes (with a factor α^2 removed) at $\theta = \pi/4$, for the $i = j = 2$ case in the $AD(fg5)_1$ -model [24].